Journal of Marine Science and Application (2025) 24: 984-997
https://doi.org/10.1007/s11804-025-00673-w

RESEARCH ARTICLE

Pitch Motion Analysis of a Submerged Cylindrical Structure in a Two-layer Fluid

Champak Kr. Neog[1] **and Mohammad Hassan**[1]

Received: 27 June 2024 / Accepted: 27 September 2024

Abstract

This study investigates the effects of radiation force due to the rotational pitch motion of a wave energy device, which comprises a coaxial bottom-mounted cylindrical caisson in a two-layer fluid, along with a submerged cylindrical buoy. The system is modeled as a two-layer fluid with infinite horizontal extent and finite depth. The radiation problem is analyzed in the context of linear water waves. The fluid domain is divided into outer and inner zones, and mathematical solutions for the pitch radiating potential are derived for the corresponding boundary valve problem in these zones using the separation of variables approach. Using the matching eigenfunction expansion method, the unknown coefficients in the analytical expression of the radiation potentials are evaluated. The resulting radiation potential is then used to compute the added mass and damping coefficients. Several numerical results for the added mass and damping coefficients are investigated for numerous parameters, particularly the effects of the cylinder radius, the draft of the submerged cylinder, and the density proportion between the two fluid layers across different frequency ranges. The major findings are presented and discussed.

Keywords Pitch radiation; Eigenfunction expansion; Two-layer; Hydrodynamic coefficients; Submerged cylinder; Bottom-mounted cylinder

1 Introduction

The dynamics of a two-layer fluid system, where one fluid layer is separated from another by the density difference, are crucial for understanding complex phenomena such as stratified turbulence and density-driven flows in shallow water. This system frequently simulates environments such as estuaries, river deltas, and coastal regions, where a denser fluid (seawater) is covered by a lighter, less dense fluid (freshwater). Researchers can gain insights into wave propagation, pollutant dispersion, and mixing processes by examining the wave interaction among these layers. Mathematical modeling and simulations of two-layer fluids are crucial for predicting interactions between these layers, which is necessary for effective environmental management, infrastructure design, and assessing the impacts of climate change on coastal systems.

The study of pitch motion in a floating cylinder within a two-layer fluid system is driven by a wide range of practical and theoretical interests. This phenomenon is essential for enhancing the stability and design of marine structures, such as floating wind turbines and offshore platforms, which frequently interact with layered fluid environments. The pitch motion refers to how the cylinder tilts and oscillates around its y-axis in response to waves, offering valuable information on energy transfer efficiency and the potential for resonance or instability. Furthermore, this research contributes to the behavior prediction of such structures in real-world scenarios, where wave patterns and fluid densities may vary. Thus, this research is crucial for improving the performance and safety of marine engineering structures.

Providing considerable attention to hydrodynamic parameters when constructing offshore building projects is crucial to ensure safety. Over the past few decades, most experiments on wave loads and hydrodynamic properties for offshore buildings have focused on homogeneous fluid. However, due to variations in water depth, temperature, and

Article Highlights

- Here, we consider a two-layer fluid system with a cylindrical buoy floating vertically in the upper layer and a cylindrical plate coaxially located at the bottom
- A two-layer flow propagates waves in two modes, namely surface waves and internal waves, both of which are affected by hydrodynamic forces.
- Studied the convergence of the obtained results, evaluated the velocity potentials in pitch mode of motion, added mass and damping coefficients, and transmission and reflection coefficients.
- An analysis of how surface and internal modes of waves are affected by radii, drafts, and depth ratios are presented.
- A comparison was made between the obtained results and the established results, and found good agreement between them, and all the results were plotted graphically.

✉ Mohammad Hassan
mdhassan000@gmail.com

[1] Department of Mathematics and Scientific Computing, Madan Mohan Malaviya University of Technology Gorakhpur, Uttar Pradesh 273010, India

salt saturation, the ocean often exhibits stratification with layers of fluid of different densities. This stacking effect may substantially affect how deep-sea platform devices are used. Density stratification in aquatic environments can be effectively modeled as a two-layer fluid system. Considering its uniform shape, the cylindrical floating body is a structural form that is frequently used on different offshore buildings. The separation of variables and eigenfunction expansion methods can be applied to derive the analytical solution for the hydrodynamic forces acting on such oscillating structures using potential theory. Most previous research on water wave problems has focused on homogeneous fluids.

Bhatta and Rahman (2003) provided a mathematical derivation of the scattering and radiation phenomena associated with a cylinder in water of finite depth. Wu et al. (2004) introduced a wave energy apparatus comprising a floating buoy attached to a base-mounted caisson. They also used the separation of variables to generate mathematical solutions for different hydrodynamic forces. Using the same methodology, Wu et al. (2006) examined a different wave energy apparatus comprising two vertical cylinders with a common axis and varying radii. They employed scattering and radiation potentials, acquired through the eigenfunction expansion approach, to assess the exciting forces/moments, as well as the hydrodynamic coefficients. Shen et al. (2005) investigated a rectangular structure floating on a free surface using a semi-analytical method to explore the effects of a bottom sill on hydrodynamic coefficients, wave forces, and reflection and transmission coefficients. Martha and Bora (2007) conducted a detailed investigation on the reflection and transmission coefficient, focusing on the scattering caused by a seabed with tiny undulations. Mohapatra et al. (2024) investigated a three-dimensional mathematical hydrodynamic model connected with surface wave radiation from a floating rectangular box-type structure. Their study was based on small-amplitude water wave theory and linear structural response in finite water depths.

In contrast to studies on homogeneous fluids, investigations on two-layer fluids and their effects on wave forces and hydrodynamic properties are still in their early stages. Baines (1995) investigated the behavior of topographic impacts on fluids with density layers in his work. Within a stratified system, internal waves propagate through the interface between fluid layers when disrupted. These internal waves have been observed to occasionally exert considerable hydrodynamic forces on offshore buildings. Linton and McIver (1995) examined the two-dimensional radiation and diffraction problem in a two-layer fluid with an infinite lower layer and a finite top layer. They found that when a cylindrical object is positioned in the lower fluid layer, no wave reflection of any frequency exists in such a system. Cadby and Linton (2000) used the multipole expansion method to address the wave scattering and radiation problem of a sinking spherical object in a two-layer fluid system with an infinite bottom layer. They found that two different wave modes, namely surface and internal-wave modes, are produced by water waves in a two-layer fluid. Sturova (1999) studied the dense fluid motion induced by an oscillating circular cylinder by applying the multipole expansion technique. The multipole expansion approach was applied in that study to address the scattering and radiation problem of the internal wave arising from a mounted cylinder to the movement of dense fluid. Du et al. (2001) performed a comprehensive study on the development and propagation of internal waves, which are common in the ocean. Sherief et al. (2003) used a permeable wavemaker, vertically immersed in a two-layer fluid with a free surface on top, to compute a BVP for velocity potential based on Taylor's wavemaker theory. Using the boundary integral-equation approach, Ten and Kashiwagi (2004) obtained quantitatively conclusive results on the hydrodynamics of a floating body in a two-layer fluid with restricted depth. You et al. (2005) demonstrated the influence of density stratification on the hydrodynamic characteristics of a large-diameter cylinder.

You et al. (2005) examined the loads of reflection and transmission waves using a narrow vertical barrier in a two-layer fluid. They found that stratification drastically affects reflection and transmission forces, especially when the barrier is positioned in the interface. Shi et al. (2006) used analytical calculations to determine the wave loads and moments on a submerged rectangular box, demonstrating density stratification effects in a two-layer fluid. In a two-layer fluid framework, where the upper fluid layer is bounded by a free surface, and the lower fluid layer is enclosed by an impermeable stiff bed, a cylindrical structure mounted at the bottom generates scattering waves of only the corresponding mode of the incident wave. In contrast, the structure itself generates radiation waves of both modes. Using the multipole expansion method, Das and Mandal (2007) investigated wave scattering by a horizontal circular cylinder in a two-layer fluid system, where the upper layer is finite and covered by ice, while the lower layer is infinite. They presented numerous effects of the ice cover on reflection and transmission coefficients. You et al. (2007) provided a theoretical model that had mathematical formulas for calculating the added mass and damping coefficients, as well as the wave exciting forces acting on a bottom-mounted circular cylinder. Shi et al. (2008) calculated the hydrodynamic loads operating on a vertical cylindrical structure submerged in a two-layer fluid system. They found that the exciting forces on a cylinder immersed vertically in a two-layer fluid also comprise the hydrodynamic loads generated by incident waves of internal and surface wave modes. Shi et al. (2009) presented a theory indicating that the oscillating movement of a sub-

merged cylinder in a two-layer fluid generates two separate modes of wave numbers: the surface wave and internal wave modes. Das and Mandal (2010) examined the radiation problem for the sway and heave motions of a submerged sphere in a two-layer fluid system comprising a finite upper layer with an ice cover and an infinite lower layer of salt water. They presented graphical results for the hydrodynamic coefficients associated with this setup. Mohapatra and Bora (2010) investigated the water wave radiation problem by immersing a spherical object in a two-layer, ice-covered fluid at a finite depth. Xu and Lu (2010) introduced series solutions based on matching eigenfunction expansion to model the hydro-elastic interaction of gravity waves associated with finite and semi-infinite plates submerged horizontally in a two-layer fluid system at finite depth. Koo (2010) developed a numerical wave tank, which generated varying proportions of amplitudes corresponding to the top and bottom elevations across a range of parameters. The numerical wave tank was based on the boundary element technique and was designed to represent a two-layer fluid with an open surface in the time domain. Mohapatra and Bora (2011) explored water waves through a channel in a two-layer fluid with an undulating bottom, investigating the reflection and transmission coefficient associated with this setup. Mondal and Sahoo (2012) found that the presence of floating ice sheets does not influence the internal wave mode properties in a two-layer fluid. However, the condensing force affects the surface wave mode wave features in deep water. In terms of higher-order boundary conditions derived from a second-order PDE, Das (2015) considered a general problems involving density-stratified two-layer fluids with ice covers. Abbas et al. (2021) studied the rotating flow of a two-layer fluid comprising one viscous layer and a magnetite-water ferrofluid in a channel using the perturbation technique. Considering natural and industrial phenomena involving the interactions of two fluid layers, Shah et al. (2021) conducted a theoretical and experimental study on the dynamics of two-layer viscous fluid flows over inclined surfaces. Barman et al. (2024) established a mathematical model to study gravity wave scattering in a two-layer fluid using the matching eigenfunction expansion method. Using the solution of the diffraction problem, Neog and Hassan (2023) calculated the wave exciting force and moment of a floating cylinder in a two-layer fluid within a bottom-fitted cylinder. They also examined the impact of hydrodynamic forces on the surge radiation of a submerged buoy in a two-layer fluid with an installed second cylinder in Neog and Hassan (2024).

This study focuses on two coaxial cylinders in a two-layer fluid system with a finite depth: one cylinder is bottom-mounted, and the other is floating rotationally around the y-axis. The authors believe that studies on two coaxial vertical cylinders in a two-layer fluid with a finite depth using the applied methodology have not yet been conducted. Wu et al. (2004) examined the diffraction and radiation problems on such devices in a homogeneous fluid only. The present study aims to provide contributions to the understanding of wave phenomena, focusing on hydrodynamic coefficients associated with the pitch motion of the device, in relation to various physical parameters.

Section 1 presents an overview of the importance and the relevant literature of fluid structure interaction. Section 2 formulates the boundary value problem along with the boundary conditions associated with the pitch motion of the device in the two-layer fluid system. The entire fluid domain is divided into two zones: interior and exterior zones. Section 3 derives the analytical expressions of the pitch radiating potential in both zones using the variable separation method. The next step is to determine the values of the unknown coefficients arising in the radiating potential using the matched eigenfunction expansion method. Section 4 evaluates the added mass and damping coefficient related to pitch motion using linearized Bernoulli's equation to determine the forces on the device. Section 5 graphically presents their behavior for different sets of parameters across a specific frequency range. Section 6 presents the conclusion, which discusses the results, importance, and future prospects of the present work.

2 Governing equation and applicable boundary constraints

This study focuses on a two-layer fluid system, where the upper fluid layer is bounded by an open surface on the top, and the lower layer is confined by a hard, impenetrable base at the bottom. The horizontal breadth of the fluid layer is infinite. An interface separates the fluid layers. The fluid densities of the top and bottom layers are denoted by ρ_1, ρ_2, and h_1, h_2, respectively, corresponding to the respective depths. The ratio of the density ρ_1/ρ_2 between the two fluid layers is γ, and the total depth from the open surface to the hard base is h, i.e., $h = h_1 + h_2$.

This study explores the radiation problem caused by small rotational pitch oscillations of a vertically submerged cylinder that extends through the open surface, with a bottom-mounted coaxial cylinder placed in the lower fluid layer. Assume the presence of minute rotational pitch oscillations at frequency ω in the floating cylinder. The Cartesian system (x, y, z) shows that the (x, y)-plane is aligned with the unperturbed open surface and the z-axis is aligned with the cylinder's axis in an upward direction, as presented in Figure 1. Each fluid layer exhibits infinitely in the horizontal directions of the x- and y-axes, whereas the negative z-axis determines the depth of the considered fluid system. The cylindrical coordinates (r, θ, z) are considered, as illustrated in Figure 2, and determined as $x =$

$r\cos\theta$, $y = r\sin\theta$ and $z = z$. The radii of cylinders are represented as b, the draft of the upper cylinder is d_1, and the distance between the top of the mounted cylinder and the open surface is denoted as d_2. It is considered that the fluid in both layers is inviscidand flows irrotationally, with gravity inducing surface and internal waves with sufficiently small amplitudes.

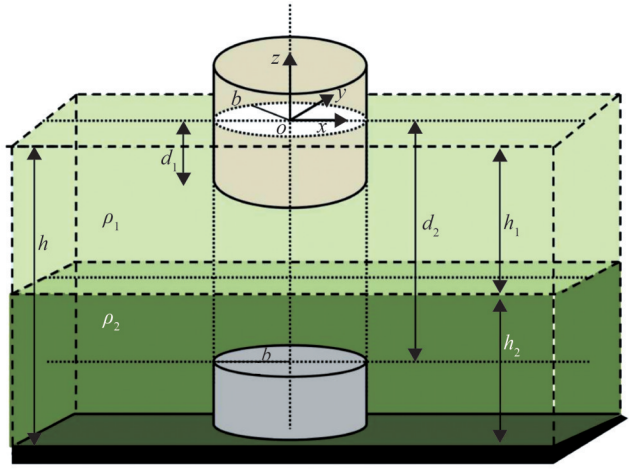

Figure 1 Diagrammatic presentation of the device in both fluid layers

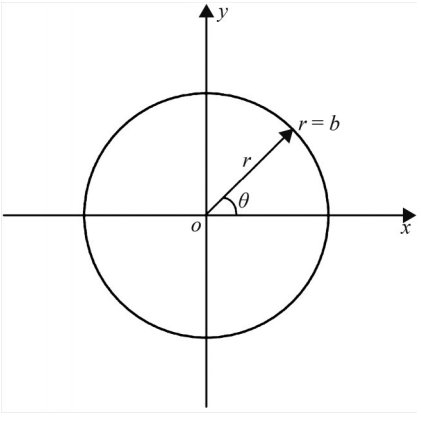

Figure 2 Consideration of polar and Cartesian coordinate systems

This study aims to investigate the rotating pitch motion of the submerged cylinder. The pitch radiation potential is depicted as follows:

$$\Phi^{s}_{\text{rad},5}(r,\theta,z,t) = \text{Re}\left[\phi^{s}_{\text{rad},5}(r,\theta,z)\,\text{e}^{-\text{i}\omega t}\right] \tag{1}$$

where $i = \sqrt{-1}$, and the sign Re denotes the real component of the associated function. The superscripts $s = 1, 2$ denote the upper and bottom fluid layers, respectively. The function $\phi^{s}_{\text{rad},5}(r,\theta,z)$ satisfies Laplace's formula:

$$\nabla^2\phi^{s}_{\text{rad},5}(r,\theta,z) = 0 \tag{2}$$

That is,

$$\frac{1}{r}\frac{\partial}{\partial r}\left(r\frac{\partial\phi^{s}_{\text{rad},5}}{\partial r}\right) + \frac{1}{r^2}\frac{\partial^2\phi^{s}_{\text{rad},5}}{\partial\theta^2} + \frac{\partial^2\phi^{s}_{\text{rad},5}}{\partial z^2} = 0$$

The aforementioned is the governing equation of the suggested pitch radiation problem.

As stated by Wu et al. (2006), if the device under consideration undergoes small pitch oscillation, then the radiation velocity potential along with amplitude $\psi_1^{(s)}$ can be divided as follows:

$$\phi^{s}_{\text{rad},5}(r,\theta,z) = -\text{i}\omega\psi_1^{(s)}\varphi^{s}_{\text{rad},5}(r,z)\cos\theta \tag{3}$$

where $\varphi^{s}_{\text{rad},5}(r,z)$ is the spatial radiation potential generated by the pitch oscillation motion of the floating cylinder. This BVP can be inverted into free from θ by substituting Eq. (2) with Eq. (3); that is,

$$\frac{1}{r}\frac{\partial\varphi^{s}_{\text{rad},5}}{\partial r} + \frac{\partial^2\varphi^{s}_{\text{rad},5}}{\partial r^2} + \frac{\partial^2\varphi^{s}_{\text{rad},5}}{\partial z^2} - \frac{\varphi^{s}_{\text{rad},5}}{r^2} = 0 \tag{4}$$

Furthermore, the linearized boundary constraints can be depicted as follows (Neog and Hassan (2024)):

• Open surface condition:

$$\frac{\partial\varphi^{1}_{\text{rad},5}}{\partial z} = K\varphi^{1}_{\text{rad},5},\ \text{on}\ z = 0 \tag{5}$$

• Hard-based bottom condition:

$$\frac{\partial\varphi^{2}_{\text{rad},5}}{\partial z} = 0,\ \text{on}\ z = -h \tag{6}$$

• Interface conditions:

$$\frac{\partial\varphi^{1}_{\text{rad},5}}{\partial z} = \frac{\partial\varphi^{2}_{\text{rad},5}}{\partial z},\ \text{on}\ z = -h_1 \tag{7}$$

$$\gamma\left(\frac{\partial\varphi^{1}_{\text{rad},5}}{\partial z} - K\varphi^{1}_{\text{rad},5}\right) = \frac{\partial\varphi^{2}_{\text{rad},5}}{\partial z} - K\varphi^{2}_{\text{rad},5},\ \text{on}\ z = -h_1 \tag{8}$$

• Far-field condition:

$$\lim_{r\to\infty}\sqrt{r}\left(\frac{\partial\varphi^{s}_{\text{rad},5}}{\partial r} \pm \text{i}k\varphi^{s}_{\text{rad},5}\right) = 0 \tag{9}$$

where g represents the acceleration caused by gravity, and $K = \omega^2/\text{g}$. Equations (7) and (8) denote the continuity of pressure and normal velocity at the interface, respectively. The problem domain is partitioned into two zones, as presented in Figure 1;

$$\xi_1 = \left\{(r,\theta,z)\,\middle|\, r \geqslant b, \theta \in [0, 2\pi), -h \leqslant z \leqslant 0\right\} \tag{10}$$

$$\xi_2 = \left\{(r,\theta,z)\,\middle|\, r < b, \theta \in [0, 2\pi), -d_2 \leqslant z \leqslant -d_1\right\} \tag{11}$$

Consider $\varphi_{\text{rad, 5}}^{(s,\text{ext})}$ and $\varphi_{\text{rad, 5}}^{(s,\text{int})}$ as the pitch radiated velocity potentials that correspond to the exterior region ξ_1 and interior region ξ_2, respectively. These velocity potentials satisfy the following body boundary conditions for the device, particularly for the pitch rotational motion of the submerged cylinder:

$$\frac{\partial \varphi_{\text{rad, 5}}^{(s,\text{ext})}}{\partial r} = z, \text{ on } r = b, \text{ in } -d_1 \leqslant z \leqslant 0 \tag{12}$$

$$\frac{\partial \varphi_{\text{rad, 5}}^{(s,\text{ext})}}{\partial r} = 0, \text{ on } r = b, \text{ in } -h \leqslant z \leqslant -d_2 \tag{13}$$

Along the z-direction in the interior region of the submerged cylinder, two different kinds of body boundary conditions are available, namely homogeneous and particular conditions, in terms of rotational pitch motion. The homogeneous condition is given by:

$$\frac{\partial \varphi_{\text{rad, 5}}^{(s,\text{int})}}{\partial z} = 0, \text{ on } r \leqslant b, \text{ in } z = -d_1, z = -d_2 \tag{14}$$

and the particular conditions are given by the following:

$$\frac{\partial \varphi_{\text{rad, 5}}^{(s,\text{int})}}{\partial z} = -r, \text{ on } 0 \leqslant r \leqslant b, \text{ in } z = -d_1 \tag{15}$$

$$\frac{\partial \varphi_{\text{rad, 5}}^{(s,\text{int})}}{\partial z} = 0, \text{ on } 0 \leqslant r \leqslant b, \text{ in } z = -d_2 \tag{16}$$

The rotational pitch motion of the submerged cylinder yields two distinct wave numbers, namely $k_0^{(1)}$ and $k_0^{(2)}$, which correspond to the surface wave and internal wave modes, respectively, in the two-layer fluid system under investigation. $k_0^{(1)}$ and $k_0^{(2)}$ can be calculated by considering the positive roots of the subsequent dispersion relations (Neog and Hassan (2024)):

$$2\frac{\omega^2}{gk}\left(1 + \gamma\tau_1\tau_2\right) = \tau_1 + \tau_2 + \sqrt{\left(\tau_1 + \tau_2\right)^2 - 4\varepsilon\tau_1\tau_2\left(1 + \gamma\tau_1\tau_2\right)} \tag{17}$$

$$2\frac{\omega^2}{gk}\left(1 + \gamma\tau_1\tau_2\right) = \tau_1 + \tau_2 - \sqrt{\left(\tau_1 + \tau_2\right)^2 - 4\varepsilon\tau_1\tau_2\left(1 + \gamma\tau_1\tau_2\right)} \tag{18}$$

where, $\tau_1 = \tanh\left(kh_1\right)$, $\tau_1 = \tanh\left(kh_1\right)$, and $\varepsilon = 1 - \gamma$

3 Rotational pitch potential

The separation of variables approach provides a mathematical solution for pitch radiating velocity potentials in either of the fluid layers in the relevant zones. The analytical formulations of the pitch radiating potentials, namely $\varphi_{\text{rad, 5}}^{(s,\text{ext})}$ and $\varphi_{\text{rad, 5}}^{(s,\text{int})}$, are derived for the exterior region ξ_1 and the interior region ξ_2, respectively. The rotational pitch of a two-layer fluid can be developed through two modes: the internal wave mode and the surface wave mode. Thus, for every fluid layer $\left(s = 1, s = 2\right)$ in the outer zone ξ_1, the mathematical expression of the pitch radiating potentials $\varphi_{\text{rad, 5}}^{(s,\text{ext})}$ is analytically obtained as follows:

$$\begin{aligned}\varphi_{\text{rad, 5}}^{(s,\text{ext})}(r,z) = {} & C_{0,1}\bar{H}_1\left(k_0^{(1)}, r\right)Z^{(s)}\left(k_0^{(1)}, z\right) + \\ & C_{0,2}\bar{H}_1\left(k_0^{(2)}, r\right)Z^{(s)}\left(k_0^{(2)}, z\right) + \\ & \sum_{m=1}^{\infty} C_{m,1}\bar{K}_1\left(k_m^{(1)}, r\right)Z^{(s)}\left(\bar{k}_m^{(1)}, z\right) + \\ & \sum_{m=1}^{\infty} C_{m,2}\bar{K}_1\left(k_m^{(2)}, r\right)Z^{(s)}\left(\bar{k}_m^{(2)}, z\right)\end{aligned} \tag{19}$$

where the vertical eigenfunctions can be expressed as follows:

$$Z^{(1)}(k,z) = \frac{\frac{\omega^2}{gk}\sinh(kz) + \cosh(kz)}{\cosh\left(kh_1\right)\left\{1 - \frac{gk}{\omega^2}\tanh\left(kh_1\right)\right\}} \tag{20}$$

$$Z^{(2)}(k,z) = \frac{\omega^2}{gk\sinh\left(kh_2\right)}\cosh\left(k\left(z + h\right)\right) \tag{21}$$

and the radial eigenfunctions are $\bar{H}_1\left(k_0^{(t)}, r\right) = \frac{H_1^{(1)}\left(k_0^{(t)}, r\right)}{H_1^{(1)}\left(k_0^{(t)}, b\right)}$, $\bar{K}_1\left(k_m^{(t)}, r\right) = \frac{K_1\left(k_m^{(t)}, r\right)}{K_1\left(k_m^{(t)}, b\right)}$, $t = 1, 2$, $m = 1, 2, 3, \cdots$ $H_1^{(1)}$ is the first kind of Hankel function of order 1, and K_1 is the Macdonald function of order 1. $\bar{k}_m^{(t)} = ik_m^{(t)}$, where $k_m^{(1)}$ and $k_m^{(2)}$ can be computed from the subsequent dispersion relations:

$$2\frac{\omega^2}{gk}\left(1 - \gamma\sigma_1\sigma_2\right) = -\left\{\sigma_1 + \sigma_2 + \sqrt{\left(\sigma_1 + \sigma_2\right)^2 - 4\varepsilon\sigma_1\sigma_2\left(1 - \gamma\sigma_1\sigma_2\right)}\right\} \tag{22}$$

$$2\frac{\omega^2}{gk}\left(1 - \gamma\sigma_1\sigma_2\right) = -\left\{\sigma_1 + \sigma_2 - \sqrt{\left(\sigma_1 + \sigma_2\right)^2 - 4\varepsilon\sigma_1\sigma_2\left(1 - \gamma\sigma_1\sigma_2\right)}\right\} \tag{23}$$

where $\sigma_1 = \tan\left(kh_1\right)$, $\sigma_2 = \tan\left(kh_2\right)$. In Eq. (19), radiating waves are represented by the first two terms, while the remaining terms represent the disturbing potentials of the surface- and internal-wave mode modes, respectively.

The velocity potential in the interior zone of the rotational pitch motion comprises two parts: the homogeneous solution and the particular solution, that is:

$$\varphi_{\text{rad, 5}}^{(s,\text{int})} = \varphi_{\text{rad, 5}}^{(s,\text{hom})} + \varphi_{\text{rad, 5}}^{(s,\text{part})} \tag{24}$$

Using the boundary condition given by Eq. (14), the homogeneous part of the pitch radiated velocity potential $\varphi_{\text{rad, 5}}^{(s,\text{hom})}$ is also derived through the same method in the interior region ξ_2, which takes the following form:

$$\varphi_{\text{rad, 5}}^{(s,\text{hom})}(r,z) = \sum_{n=0}^{\infty} W_n R_1(\lambda_n, r) Y^{(s)}(\lambda_n, z) \tag{25}$$

Using the corresponding boundary conditions mentioned in (15) and (16), the particular solution is determined as follows:

$$\varphi_{\text{rad, 5}}^{(s,\text{part})}(r,z) = \begin{cases} D\left[\dfrac{r^3}{8} - \dfrac{(z+d_2)^2 r}{2} - (1-\gamma)h_2 zr\right], \\ \quad \text{for the region } -h_1 \leqslant z \leqslant -d_1 \\ \gamma D\left[\dfrac{r^3}{8} - \dfrac{(z+d_2)^2 r}{2} - (1-\gamma)\left(\dfrac{g}{\omega^2} + h_1\right) r h_2\right], \\ \quad \text{for the region } -d_2 \leqslant z \leqslant -h_1 \end{cases} \tag{26}$$

where $D = \dfrac{1}{(d_2 - d_1) - (1-\gamma)h_2}$.

The vertical eigenfunctions $Y^{(s)}(\lambda_n, z)$ of Eq. (25) for the respective fluid layers, i.e., $s = 1$ in the upper layer fluid $(-h_1 \leqslant z \leqslant -d_1)$ and $s = 2$ in the lower fluid layer $(-d_2 \leqslant z \leqslant -h_1)$, can be respectively expressed as follows:

$$Y^{(1)}(\lambda_n, z) = \begin{cases} 1, & n = 0 \\ \dfrac{\sinh(\lambda_n(d_2 - h_1))}{\cosh(\lambda_n d_2)\sinh(\lambda_n(d_1 - h_1))}\cosh(\lambda_n(z + d_1)), & n = 1 \\ \cos(\lambda_n(z + d_1)), & n \geqslant 2 \end{cases} \tag{27}$$

$$Y^{(2)}(\lambda_n, z) = \begin{cases} \gamma, & n = 0 \\ \dfrac{\sinh(\lambda_n(d_1 - h_1))}{\cosh(\lambda_n d_1)\sinh(\lambda_n(d_2 - h_1))}\cosh(\lambda_n(z + d_2)), & n = 1 \\ \dfrac{\sin(\lambda_n(d_1 - h_1))}{\sin(\lambda_n(d_2 - h_1))}\cos(\lambda_n(z + d_2)) & n \geqslant 2 \end{cases} \tag{28}$$

The radial eigenfunction $R_1(\lambda_n, r)$ can be expressed as:

$$R_1(\lambda_n, r) = \begin{cases} \dfrac{r}{b}, & n = 0 \\ \dfrac{J_1(\lambda_n r)}{J_1(\lambda_n b)}, & n = 1 \\ \dfrac{I_1(\lambda_n r)}{I_1(\lambda_n b)} & n \geqslant 2 \end{cases} \tag{29}$$

where J_1 is the first kind of Bessel function of order 1, and I_1 is the first kind of modified Bessel function of order 1. Moreover, $\lambda_0 = 0$, λ_1 is the positive real root of the following equation:

$$\omega^2 = \frac{\varepsilon g \lambda \tanh(\lambda(d_2 - h_1))\tanh(\lambda(d_1 - h_1))}{\tanh(\lambda(d_1 - h_1)) - \gamma\tanh(\lambda(d_2 - h_1))} \tag{30}$$

and for $n \geqslant 2$, λ_n is calculated by solving the dispersion relation provided below:

$$\omega^2 = \frac{\varepsilon g \lambda \tan(\lambda(d_2 - h_1))\tan(\lambda(d_1 - h_1))}{\tan(\lambda(d_2 - h_1)) - \gamma\tan(\lambda(d_1 - h_1))} \tag{31}$$

3.1 Matching conditions

The unknown coefficients in the rotational pitch potential are computed by applying matching criteria, which may be derived from the continuity behavior of pressure and velocity at the imaginary borders of the two zones defined by Eqs. (10) and (11). The imaginary borderline separating the two zones is shown in Figure 1. In the imaginary boundary line of the zones ξ_1 and ξ_2, either potentials $\varphi_{\text{rad, 5}}^{(s,\text{ext})}$ and $\varphi_{\text{rad, 5}}^{(s,\text{int})}$ fulfill these matching conditions as depicted below:

$$\varphi_{\text{rad, 5}}^{(s,\text{ext})} = \varphi_{\text{rad, 5}}^{(s,\text{int})}, \text{ in } -d_2 \leqslant z \leqslant -d_1,\ r = b \tag{32}$$

$$\left.\frac{\partial \varphi_{\text{rad, 5}}^{(s,\text{ext})}}{\partial r}\right|_{r=b} = \begin{cases} 0, & (-d_1 \leqslant z \leqslant 0) \\ \left.\dfrac{\partial \varphi_{\text{rad, 5}}^{(s,\text{int})}}{\partial r}\right|_{r=b}, & (-d_2 \leqslant z \leqslant -d_1) \\ 0, & (-h \leqslant z \leqslant -d_2) \end{cases} \tag{33}$$

3.2 Unknown coefficients

The observation indicates that the unknown coefficients are $C_{m,t}$ and W_n, in the derived pitch radiating potentials in exterior and interior regions, the matching criteria provided by Eqs. (32) and (33) are used to compute these unknown coefficients. Using the rotating pitch velocity potentials in

the appropriate zones satisfying the matching requirements, the following equations are obtained:

$$\sum_{m=0}^{\infty} C_{m,1} Z^{(s)}\left(\overline{k_m^{(1)}}, z\right) + \sum_{m=0}^{\infty} C_{m,2} Z^{(s)}\left(\overline{k_m^{(2)}}, z\right) = \sum_{n=0}^{\infty} W_n Y^{(s)}\left(\lambda_n, z\right) + \varphi_{\text{rad},5}^{(s,\text{part})}(b, z), \quad \text{in the region } -d_2 \leqslant z \leqslant -d_1 \tag{34}$$

and,

$$\begin{aligned} & k_0^{(1)} C_{0,1} \overline{H_1}'\left(k_0^{(1)}, b\right) Z^{(s)}\left(k_0^{(1)}, z\right) + \\ & \quad k_0^{(2)} C_{0,2} \overline{H_1}'\left(k_0^{(2)}, b\right) Z^{(s)}\left(k_0^{(2)}, z\right) + \\ & \quad k_m^{(1)} \sum_{m=1}^{\infty} C_{m,1} \overline{K_1}'\left(k_m^{(1)}, b\right) Z^{(s)}\left(\overline{k_m^{(1)}}, z\right) + \\ & \quad k_m^{(2)} \sum_{m=1}^{\infty} C_{m,2} \overline{K_1}'\left(k_m^{(2)}, b\right) Z^{(s)}\left(\overline{k_m^{(2)}}, z\right) = \\ & \begin{cases} 0, & -d_1 \leqslant z \leqslant 0 \\ \sum_{n=0}^{\infty} \lambda_n W_n R_1'\left(\lambda_n, b\right) Y^{(s)}\left(\lambda_n, z\right) + \\ \quad \frac{\partial}{\partial r}\left[\varphi_{\text{rad},5}^{(s,\text{part})}(r, z)\right]\Big|_{r=b}, & -d_2 \leqslant z \leqslant -d_1 \\ 0, & -h \leqslant z \leqslant -d_2 \end{cases} \end{aligned} \tag{35}$$

where $\lambda_0 = 1$.

The values obtained throughout the relevant regions of the matched boundary are integrated by multiplying orthogonal functions to Eqs. (34) and (35). Additionally, series summations are truncated to $M + 1$ and $N + 1$ items for the left-hand and right-hand series, respectively. Moreover, $\eta(z)$ is defined as

$$\eta(z) = \begin{cases} \gamma, & -h_1 \leqslant z \leqslant 0 \\ 1, & -h \leqslant z \leqslant -h_1 \end{cases} \tag{36}$$

First, $\eta(z) Y^{(s)}\left(\lambda_n, z\right)$ $(n = 0, 1, 2, \cdots, N)$ is multiplied on both sides of Eq. (34), and then integration is conducted over the zone $-d_2 \leqslant z \leqslant -d_1$. Once the series summations are truncated, all the unknowns are shifted to the left side of the equation, yielding the following:

$$\left[c_{nm}^{(1)}\right]_{(N+1)(M+1)} \left\{C_{m,1}\right\}_{M+1} + \left[c_{nm}^{(2)}\right]_{(N+1)(M+1)} \left\{C_{m,2}\right\}_{M+1} - \left\{W_n\right\}_{N+1} = \left\{e_n\right\}_{N+1} \tag{37}$$

where

$$c_{nm}^{(t)} = \frac{\int_{-d_2}^{-d_1} \eta(z) Z^{(s)}\left(\overline{k_m^{(t)}}, z\right) Y^{(s)}\left(\lambda_n, z\right) \mathrm{d}z}{\int_{-d_2}^{-d_1} \eta(z) \left[Y^{(s)}\left(\lambda_n, z\right)\right]^2 \mathrm{d}z}, \quad \overline{k_0^{(1)}} = k_0^{(1)}, \overline{k_0^{(2)}} = k_0^{(2)} \tag{38}$$

for $m = 0, 1, 2, 3, \cdots, M$, and

$$e_n = \frac{\int_{-d_2}^{-d_1} \eta(z) Y^{(s)}\left(\lambda_n, z\right) \varphi_{\text{rad},5}^{(s,\text{part})}(b, z) \mathrm{d}z}{\int_{-d_2}^{-d_1} \eta(z) \left[Y^{(s)}\left(\lambda_n, z\right)\right]^2 \mathrm{d}z} \tag{39}$$

By multiplying $\eta(z) Z^{(s)}\left(k_0^{(1)}, z\right)$, $\eta(z) Z^{(s)}\left(\overline{k_m^{(1)}}, z\right)$, $\eta(z) Z^{(s)}\left(k_0^{(2)}, z\right)$, $\eta(z) Z^{(s)}\left(\overline{k_m^{(2)}}, z\right)$, and $(m = 1, 2, 3, \cdots, M)$ on both side of Eq. (35) and operating integration over $-h \leqslant z \leqslant 0$, the second truncated series can be obtained as follows:

$$\left\{C_{m,t}\right\}_{M+1} - \left[w_{mn}^{(t)}\right]_{(M+1)(N+1)} \left\{W_n\right\}_{N+1} = \left\{f_m^{(t)}\right\}_{M+1} \tag{40}$$

where $t = 1, 2$, and,

$$f_0^{(t)} = \frac{\int_{-d_2}^{-d_1} \eta(z) Z^{(s)}\left(k_0^{(t)}, z\right) \frac{\partial}{\partial r}\left[\varphi_{\text{rad},5}^{(s,\text{part})}(r, z)\right]\Big|_{r=b} \mathrm{d}z}{k_0^{(t)} \overline{H_1}'\left(k_0^{(t)}, b\right) \int_{-h}^{0} \eta(z) \left[Z^{(s)}\left(k_0^{(t)}, z\right)\right]^2 \mathrm{d}z} \tag{41}$$

$$f_m^{(t)} = \frac{\int_{-d_2}^{-d_1} \eta(z) Z^{(s)}\left(\overline{k_m^{(t)}}, z\right) \frac{\partial}{\partial r}\left[\varphi_{\text{rad},5}^{(s,\text{part})}(r, z)\right]\Big|_{r=b} \mathrm{d}z}{k_m^{(t)} \overline{K_1}'\left(k_m^{(t)}, b\right) \int_{-h}^{0} \eta(z) \left[Z^{(s)}\left(\overline{k_m^{(t)}}, z\right)\right]^2 \mathrm{d}z}, \quad m = 1, 2, 3, \cdots, M \tag{42}$$

$$w_{0n}^{(t)} = \frac{\lambda_n R_1'\left(\lambda_n, b\right) \int_{-d_2}^{-d_1} \eta(z) Z^{(s)}\left(\overline{k_0^{(t)}}, z\right) Y^{(s)}\left(\lambda_n, z\right) \mathrm{d}z}{k_0^{(t)} \overline{H_1}'\left(k_0^{(t)}, b\right) N_0^{(t)}} \tag{43}$$

$$w_{mn}^{(t)} = \frac{\lambda_n R_1'\left(\lambda_n, b\right) \int_{-d_2}^{-d_1} \eta(z) Z^{(s)}\left(\overline{k_m^{(t)}}, z\right) Y^{(s)}\left(\lambda_n, z\right) \mathrm{d}z}{k_m^{(t)} \overline{K_1}'\left(k_m^{(t)}, b\right) N_m^{(t)}}, \quad m = 1, 2, 3, \cdots, M \tag{44}$$

$$N_m^{(t)} = \int_{-h}^{0} \eta(z) \left[Z^{(s)}\left(\overline{k_m^{(t)}}, z\right)\right]^2 \mathrm{d}z, m = 0, 1, 2, 3, \cdots, M \tag{45}$$

The pitch radiating potentials $\varphi_{\text{rad},5}^{(s,\text{ext})}$ and $\varphi_{\text{rad},5}^{(s,\text{int})}$ in the corresponding zones may be completely obtained by solving the matrices given by Eqs. (37) and (40).

4 Evaluation of hydrodynamics coefficients

The hydrodynamic coefficients associated with rotational pitch motion, such as the added mass and damping coefficients, can be derived using a linearized Bernoulli's equation, which is based on hydrodynamic pressure and radiating force, as indicated below (Shi et al. (2009)):

$$\mu_{55} + \mathrm{i}\frac{\lambda_{55}}{\omega} = b\int_{-d_1}^{0}\int_{0}^{2\pi} z\rho_s(z)\varphi_{\text{rad},5}^{(s,\text{ext})}(b,z)\left(-\cos^2\theta\right)\mathrm{d}\theta\mathrm{d}z - \rho_s(d_1)\int_{0}^{b}\int_{0}^{2\pi}\varphi_{\text{rad},5}^{(s,\text{int})}(r,-d_1)r^2\cos^2\theta\mathrm{d}\theta\mathrm{d}r \tag{46}$$

where,

$$\rho_s(z) = \begin{cases}\rho_1, & -h \leqslant z \leqslant 0\\ \rho_2, & -h \leqslant z \leqslant -h_1\end{cases} \tag{47}$$

The notation μ_{55} and λ_{55} represent the additional mass and damping coefficient, respectively, generated by the rotational pitch oscillation of the submerged cylinder. By substituting the values of $\varphi_{\text{rad},5}^{(s,\text{ext})}(b,z)$ and $\varphi_{\text{rad},5}^{(s,\text{int})}(r,-d_1)$, and evaluating the integrals, the following is provided:

$$\begin{aligned}\mu_{55} + i\frac{\lambda_{55}}{\omega} = {} & -\pi b\rho_1\int_{-d_1}^{0} z\left\{C_{0,1}Z^{(1)}\left(k_0^{(1)},z\right) + C_{0,2}Z^{(1)}\left(k_0^{(2)},z\right) + \sum_{m=1}^{\infty}C_{m,1}Z^{(1)}\left(\overline{k_m^{(1)}},z\right) + \sum_{m=1}^{\infty}C_{m,2}Z^{(1)}\left(\overline{k_m^{(2)}},z\right)\right\}\mathrm{d}z - \pi\rho_1\int_{0}^{b} r^2\left[W_0\frac{r}{b} + W_1\frac{J_1(\lambda_1 r)}{J_1(\lambda_1 b)}\frac{\sinh\left(\lambda_1(d_2-h_1)\right)}{\cosh(\lambda_1 d_2)\sinh\left(\lambda_1(d_1-h_1)\right)} + \sum_{n=2}^{\infty}W_n\frac{I_1(\lambda_n r)}{I_1(\lambda_n b)} + \mathrm{D}\left\{\frac{r^3}{8} - \frac{(d_2-d_1)^2 r}{2} + (1-\gamma)h_2 d_1 r\right\}\right]\mathrm{d}r\end{aligned} \tag{48}$$

that is,

$$\begin{aligned}\mu_{55} + i\frac{\lambda_{55}}{\omega} = {} & -\pi b\rho_1\left[C_{0,1}D^*\left(k_0^{(1)}\right) + C_{0,2}D^*\left(k_0^{(2)}\right) + \sum_{m=1}^{\infty}C_{m,1}D^*\left(\overline{k_m^{(1)}}\right) + \sum_{m=1}^{\infty}C_{m,2}D^*\left(\overline{k_m^{(2)}}\right)\right] - \pi\rho_1\left[W_0\frac{b^3}{4} + W_1\frac{\sinh\left(\lambda_1(d_2-h_1)\right)}{\cosh(\lambda_1 d_2)\sinh\left(\lambda_1(d_1-h_1)\right)}\left(\frac{2b}{\lambda_1^2} - \frac{b^2}{\lambda_1}\frac{J_0(b\lambda_1)}{J_1(b\lambda_1)}\right) + \sum_{n=2}^{\infty}W_n\left(\frac{b^2}{\lambda_n}\frac{I_0(b\lambda_n)}{I_1(b\lambda_n)} - \frac{2b}{\lambda_n^2}\right) + \mathrm{D}\left\{\frac{b^4\left(12(1-\gamma)h_2 d_1 - 6(d_2-d_1)^2 + b^2\right)}{48}\right\}\right]\end{aligned} \tag{49}$$

where,

$$D^*(k) = \frac{\left[\frac{\left\{\left(\frac{K}{k}-1\right)d_1 k - \left(\frac{K}{k}+1\right)\right\}\mathrm{e}^{d_1 k} + \left(\frac{K}{k}+1\right)(d_1 k+1)\mathrm{e}^{-d_1 k}}{2k^2} - \frac{1}{k^2}\right]}{\left[\cosh(kh_1)\left\{1 - \frac{k}{K}\tanh kh_1\right\}\right]}$$

and J_0 is the first-kind zero-order Bessel function, and I_0 is the first-kind zero-order Modified Bessel function.

Furthermore, the study on wave quantity, i.e., the reflection and transmission coefficients, must consider the scattering problem of the device. The incident wave potential is taken as shown below to consider the scattering problem (Neog and Hassan (2023)):

$$\phi_{\text{inc}}^{(s)}(r,\theta,z) = -\frac{ia\left(k_0^{(t)}\right)\mathrm{g}}{\omega}Z^{(s)}\left(k_0^{(t)},z\right)\sum_{l=0}^{\infty}\varepsilon_l i^l J_l\left(k_0^{(t)}r\right)\cos l\theta \tag{50}$$

where $\varepsilon_0 = 1$, $\varepsilon_l = 2$ for $l \geqslant 1$, and $J_l(l = 0, 1, 2, \cdots)$ are the Bessel functions of the first kind of order l, and $a\left(k_0^{(t)}\right)$ is given by

$$a\left(k_0^{(t)}\right) = \begin{cases} a_0^{(1)}\left(k_0^{(1)}\right)\cosh\left(k_0^{(1)}h_1\right)\left\{1 - \frac{\mathrm{g}k_0^{(1)}}{\omega^2}\tanh\left(k_0^{(1)}h_1\right)\right\}, & \text{for } t = 1\\ a_0^{(2)}\left(k_0^{(2)}\right), & \text{for } t = 2\end{cases} \tag{51}$$

where $a_0^{(1)}\left(k_0^{(t)}\right)$ and $a_0^{(2)}\left(k_0^{(t)}\right)$ are the amplitudes of the free surface and interface, respectively, due to the incident wave

of mode t. Eq. (50) can be rewritten as mentioned in Linton and MacIver (2001):

$$\phi_{\text{inc}}^{(s)}(x,z) = -\frac{ia\left(k_0^{(t)}\right)\text{g}}{\omega} Z^{(s)}\left(k_0^{(t)},z\right)\text{e}^{i\left(k_0^{(t)}x\right)} \tag{52}$$

The total potential of the outer zone ξ_1, which is the summation of incident potential $\phi_{\text{inc}}^{(s)}$ and diffracted potential $\phi_d^{(s)}$, is denoted by $\phi_{\text{total}}^{(s)}$ and defined as follows:

$$\begin{aligned}\phi_{\text{total}}^{(s)}(r,\theta,z) = & \\ & -\frac{ia\left(k_0^{(t)}\right)\text{g}}{\omega}\sum_{l=0}^{\infty}\varepsilon_l i^l\cos l\theta\Bigg[J_l\left(k_0^{(t)}r\right)Z^{(s)}\left(k_0^{(t)},z\right)+\\ & P_{l0}^{(t,1)}\overline{H_l}\left(k_0^{(1)},r\right)Z^{(s)}\left(k_0^{(1)},z\right)+\\ & P_{l0}^{(t,2)}\overline{H_l}\left(k_0^{(2)},r\right)Z^{(s)}\left(k_0^{(2)},z\right)+\\ & \sum_{j=1}^{\infty}P_{lj}^{(t,1)}\overline{K_l}\left(k_j^{(1)},r\right)Z^{(s)}\left(\overline{k_j^{(1)}},z\right)+\\ & \sum_{j=1}^{\infty}P_{lj}^{(t,2)}\overline{K_l}\left(k_j^{(2)},r\right)Z^{(s)}\left(\overline{k_j^{(2)}},z\right)\Bigg]\end{aligned} \tag{53}$$

where $H_l^{(1)}$ $(l = 0, 1, 2, 3, \cdots)$ are the Hankel functions of the first kind of order l, and K_l $(l = 0, 1, 2, 3, \cdots)$ are the modified Bessel functions of the second kind of order l. When the wave train passes through the structure, then one part is reflected, and the other part is transmitted. The ratios of the amplitude of the reflected and transmitted wave to that of the incident wave are termed reflection and transmission coefficients, respectively. Shen et al. (2005) and Mohapatra et al. (2024) found that the reflected wave is equal to the diffracted wave along the direction $x \to -\infty$, while transmitted wave is equal to the diffraction wave along the direction $x \to \infty$ plus that of the incident wave. Notably, two modes of diffraction potential corresponding to two wave numbers, namely $k_0^{(1)}$ and $k_0^{(2)}$, are available. The reflection and transmission coefficients due to the diffraction wave of mode t are denoted by Rt and Tt, respectively. Thus, reflection and transmission coefficients for the wave mode $k_0^{(1)}$ can be obtained due to the incident wave of surface wave mode as

$$\text{R1} = \left|\frac{P_{00}^{(1,1)}}{H_0\left(k_0^{(1)}a\right)}\right| \tag{54}$$

$$\text{T1} = \left|1+\frac{P_{00}^{(1,1)}}{H_0\left(k_0^{(1)}a\right)}\right| \tag{55}$$

Similarly, the reflection and transmission coefficients for the wave mode $k_0^{(2)}$ due to the incident wave of surface wave mode can be obtained as follows:

$$\text{R2} = \left|\frac{P_{00}^{(1,2)}\cosh\left(k_0^{(1)}h_1\right)\left\{1-\frac{\text{g}k_0^{(1)}}{\omega^2}\tanh\left(k_0^{(1)}h_1\right)\right\}}{H_0\left(k_0^{(2)}a\right)\cosh\left(k_0^{(2)}h_1\right)\left\{1-\frac{\text{g}k_0^{(2)}}{\omega^2}\tanh\left(k_0^{(2)}h_1\right)\right\}}\right| \tag{56}$$

$$\text{T2} = \left|1+\frac{P_{00}^{(1,2)}\cosh\left(k_0^{(1)}h_1\right)\left\{1-\frac{\text{g}k_0^{(1)}}{\omega^2}\tanh\left(k_0^{(1)}h_1\right)\right\}}{H_0\left(k_0^{(2)}a\right)\cosh\left(k_0^{(2)}h_1\right)\left\{1-\frac{\text{g}k_0^{(2)}}{\omega^2}\tanh\left(k_0^{(2)}h_1\right)\right\}}\right| \tag{57}$$

5 Numerical results

The expressions of the radiating potentials ($\varphi_{\text{rad},5}^{(s,\text{ext})}$ and $\varphi_{\text{rad},5}^{(s,\text{int})}$) obtained in the exterior and interior zones reveal that the effects of various parameters on the added mass (μ_{55}) and damping coefficient (λ_{55}) can be investigated using Eq. (46). The effects on μ_{55} and λ_{55} due to parameters, such as radii of the contemplated cylinders (b), the draft of the submerged cylinder (d_1), and the density proportion, on both fluid layers (γ), are observed. Herein, some numerical findings for μ_{55} and λ_{55} with respect to the mentioned parameters over a frequency range are presented. In each of the cases, $\pi\rho_1 b^3 h^2$ and $\pi\omega\rho_1 b^3 h^2$ are used to nondimensionalize correspondingly the added mass and damping coefficients, respectively, while nondimensionalizes the angular frequency.

5.1 Convergence study

Notably, the linear system in Eqs. (37) and (40) was truncated during the solution process. The computation results for nondimensionalized added mass and damping coefficients corresponding to different angular frequencies with a certain number of truncated terms on the base of obtained mathematical solutions are displayed in Tables 1 and 2. The tables indicate that this solution trend is approaching convergence. Truncation of up to 30 items reveals an accuracy of up to seven digits after decimal.

5.2 Validation

The findings of this study are compared with results previously established by Shi et al. (2009), where the lower cylinder was absent, for validation. Consequently, the model measurements must be re-computed to obtain the same geometrical structure. The new parameters that are considered are as follows: $b = (5/10)\,h$, $d_1 = (5/10)\,h$, $d_2 = (9.999\,999\,9/10)\,h$, $\gamma = 0.97$. Using this set of values, Figures 3 and 4 compare the results of the present work with the established outcomes of Shi et al. (2009). The

Table 1 Convergence analysis of the nondimensionalized added mass μ_{55} due to pitch oscillation for various iteration counts in Eqs. (37) and (40), where $h_1 : h_2 = 7:3$, $\gamma = 0.97$, $b:h = 1:2$, and $d_1 : d_2 = 5:8$

$\omega\sqrt{\frac{h}{g}}$	$(M+1, N+1)$	μ_{55}	$\omega\sqrt{\frac{h}{g}}$	$(M+1, N+1)$	μ_{55}
0.06	(5, 5)	0.479 863 42	0.25	(5, 5)	0.017 639 63
	(8, 8)	0.485 923 85		(8, 8)	0.016 432 57
	(12, 12)	0.493 466 01		(12, 12)	0.015 593 48
	(16, 16)	0.493 518 74		(16, 16)	0.015 589 53
	(22, 22)	0.493 518 76		(22, 22)	0.015 589 56
	(30, 30)	0.493 518 76		(30, 30)	0.015 589 56
0.53	(5, 5)	0.015 778 45	0.79	(5, 5)	0.016 537 83
	(8, 8)	0.016 345 86		(8, 8)	0.018 485 62
	(12, 12)	0.016 554 67		(12, 12)	0.019 645 73
	(16, 16)	0.016 555 11		(16, 16)	0.019 626 38
	(22, 22)	0.016 555 23		(22, 22)	0.019 626 45
	(30, 30)	0.016 555 24		(30, 30)	0.019 626 45
1.06	(5, 5)	0.027 658 39	1.59	(5, 5)	0.034 945 38
	(8, 8)	0.024 587 36		(8, 8)	0.032 547 68
	(12, 12)	0.023 264 95		(12, 12)	0.030 549 53
	(16, 16)	0.023 265 86		(16, 16)	0.030 548 74
	(22, 22)	0.023 265 75		(22, 22)	0.030 548 68
	(30, 30)	0.023 265 75		(30, 30)	0.030 548 67
2.11	(5, 5)	0.010 385 64	2.38	(5, 5)	0.008 534 80
	(8, 8)	0.009 564 37		(8, 8)	0.008 197 20
	(12, 12)	0.006 359 33		(12, 12)	0.006 491 01
	(16, 16)	0.006 361 23		(16, 16)	0.006 473 44
	(22, 22)	0.006 360 58		(22, 22)	0.006 473 46
	(30, 30)	0.006 360 58		(30, 30)	0.006 473 46
2.64	(5, 5)	0.006 174 82	3.17	(5, 5)	0.009 215 26
	(8, 8)	0.006 729 57		(8, 8)	0.008 863 27
	(12, 12)	0.007 468 67		(12, 12)	0.008 637 08
	(16, 16)	0.007 466 38		(16, 16)	0.008 636 57
	(22, 22)	0.007 466 34		(22, 22)	0.008 636 49
	(30, 30)	0.007 466 34		(30, 30)	0.008 636 48

added mass and damping coefficient show good agreement, validating the current findings.

The quantitative findings of added mass and damping coefficients considering a range of cylinder radii, such as b/h = 5/10, 4.8/10, 4.6/10, are displayed in Figures 5 and 6. As shown in Figure 5, added mass is substantially larger in initial frequencies, but a steep decline is observed near the 0.5 point. A high radius exhibits a large added mass. The cross-sectional area exposed to the water and the pressure force distribution is affected by the radius of the cylinder. A large radius results in the displacement of additional fluid when the cylinder undergoes pitch motion, which increases the added mass. This phenomenon is due to a large radius, which generally indicates a large wetted area. In contrast, as shown in Figure 6, the damping coefficient initially increases sharply with frequency and then oscillates and gradually diminishes as the frequency continues to rise. The wave patterns produced by the pitch motion are influenced by a large radius because it increases the wetted surface. An increase in hydrodynamic damping may be attributed to this condition. The wave-making resistance acting on the cylinder determines the effect of damping coefficients. A large radius enables the use of additional surfaces for energy dissipation, thereby enhancing the damping coefficient.

Figures 7 and 8 demonstrate the graphical behavior of added mass and damping coefficient, respectively, in terms of multiple values of the draft of the floating cylinder, that is, d_1/h = 5/10, 4.5/10, 4/10. In this case, added mass and damping coefficient demonstrate a similar trend, but a greater draft notably possesses greater added mass and damping coefficient. The volume of the submerged portion of the cylinder is influenced by the draft. The added mass due to pitch motion is related to the amount of displaced water volume surrounding the cylinder, thereby requiring acceleration. With an increased draft, a larger portion of the cylinder is submerged, causing the acceleration of additional fluid due to the cylinder motion, generally resulting in an increase in the added mass. Similarly, a larger submerged area of the cylinder increases its contact with the surrounding water, leading to more energy dissipation. Therefore, a

Table 2 Convergence analysis of the nondimensionalized damping coefficient λ_{55} due to pitch oscillation for various iteration counts in Eqs. (37) and (40), where $h_1 : h_2 = 7 : 3$, $\gamma = 0.97$, $b : h = 1 : 2$, and $d_1 : d_2 = 5 : 8$

$\omega\sqrt{\frac{h}{g}}$	$(M+1, N+1)$	λ_{55}	$\omega\sqrt{\frac{h}{g}}$	$(M+1, N+1)$	λ_{55}
0.06	(5, 5)	0.014 778 94	0.25	(5, 5)	0.029 679 32
	(8, 8)	0.015 765 38		(8, 8)	0.031 563 28
	(12, 12)	0.016 201 03		(12, 12)	0.032 503 58
	(16, 16)	0.016 235 83		(16, 16)	0.032 504 73
	(22, 22)	0.016 235 67		(22, 22)	0.032 504 65
	(30, 30)	0.016 235 67		(30, 30)	0.032 504 65
0.53	(5, 5)	0.025 498 32	0.79	(5, 5)	0.010 538 74
	(8, 8)	0.022 379 84		(8, 8)	0.009 275 63
	(12, 12)	0.021 207 72		(12, 12)	0.008 716 22
	(16, 16)	0.021 208 37		(16, 16)	0.008 714 76
	(22, 22)	0.021 208 53		(22, 22)	0.008 714 68
	(30, 30)	0.021 208 53		(30, 30)	0.008 714 68
1.06	(5, 5)	0.011 975 37	1.59	(5, 5)	0.012 664 87
	(8, 8)	0.010 861 26		(8, 8)	0.014 512 98
	(12, 12)	0.010 564 66		(12, 12)	0.014 995 66
	(16, 16)	0.010 563 93		(16, 16)	0.014 996 14
	(22, 22)	0.010 563 91		(22, 22)	0.014 996 21
	(30, 30)	0.010 563 91		(30, 30)	0.0149 96 21
2.11	(5, 5)	0.012 264 83	2.38	(5, 5)	0.007 154 96
	(8, 8)	0.011 136 59		(8, 8)	0.005 659 41
	(12, 12)	0.010 387 97		(12, 12)	0.004 379 69
	(16, 16)	0.010 388 42		(16, 16)	0.004 380 27
	(22, 22)	0.010 388 38		(22, 22)	0.004 380 16
	(30, 30)	0.010 388 39		(30, 30)	0.004 380 16
2.64	(5, 5)	0.002 734 61	3.17	(5, 5)	0.000 768 44
	(8, 8)	0.001 963 95		(8, 8)	0.000 437 51
	(12, 12)	0.001 619 42		(12, 12)	0.000 347 25
	(16, 16)	0.001 618 78		(16, 16)	0.000 347 63
	(22, 22)	0.001 618 92		(22, 22)	0.000 347 72
	(30, 30)	0.001 618 93		(30, 30)	0.000 347 72

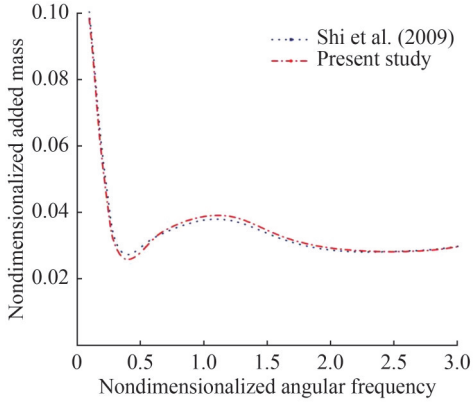

Figure 3 Comparison between the added mass calculated in this study and the SHI et al. (2009) result at $b = (5/10)\,h$, $h_1 : h_2 = 7 : 3$, $d_1 = (5/10)\,h$, $d_2 = (9.999\,999\,9/10)\,h$, and $\gamma = 0.97$

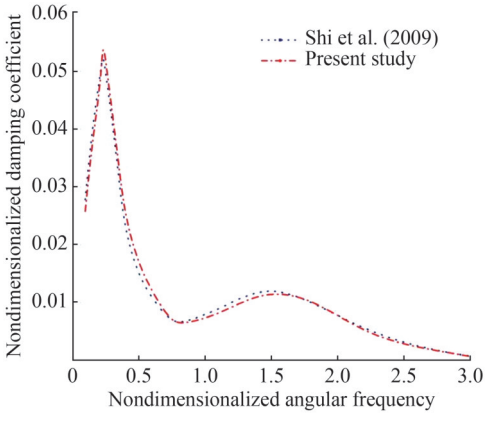

Figure 4 Comparison between the damping coefficient calculated in this study and the SHI et al. (2009) result at $b = (5/10)\,h$, $h_1 : h_2 = 7 : 3$, $d_1 = (5/10)\,h$, $d_2 = (9.999\,999\,9/10)\,h$, and $\gamma = 0.97$

deeper draft generally leads to greater hydrodynamic damping. Additional fluid is involved in the motion; thus, a large draft might eventually result in large damping.

The visual findings of added mass and damping coefficient in terms of different proportions among the fluid layers, such as $\gamma = 0.97, 0.95, 0.93$, are shown in Figures 9 and 10. Figure 9 reveals that added mass is slightly larger when the upper layer, where the cylinder undergoes oscilla-

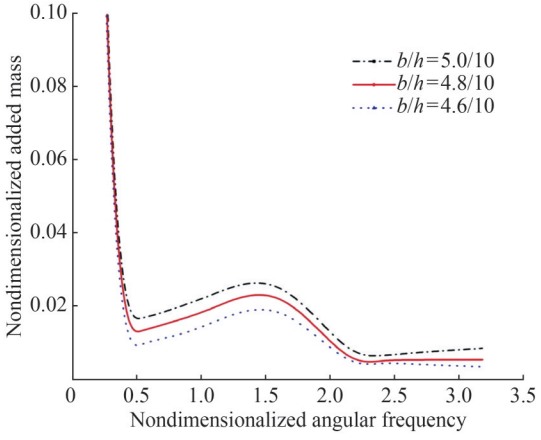

Figure 5 Added mass against angular frequency considering different cylinder radius values ($\gamma = 0.97$, $h_1 : h_2 = 7 : 3$, $d_1 : d_2 = 5 : 8$)

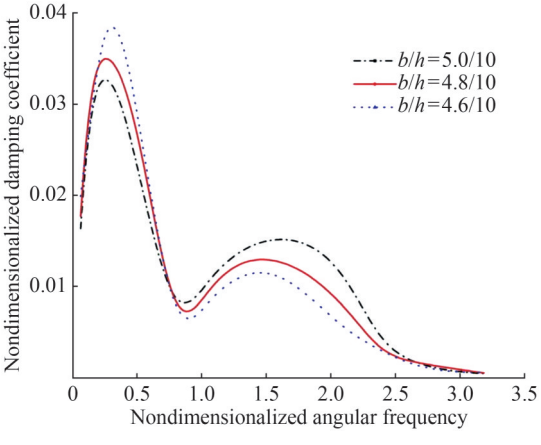

Figure 6 Damping coefficient against angular frequency considering different cylinder radius values ($\gamma = 0.97$, $h_1 : h_2 = 7 : 3$, $d_1 : d_2 = 5 : 8$)

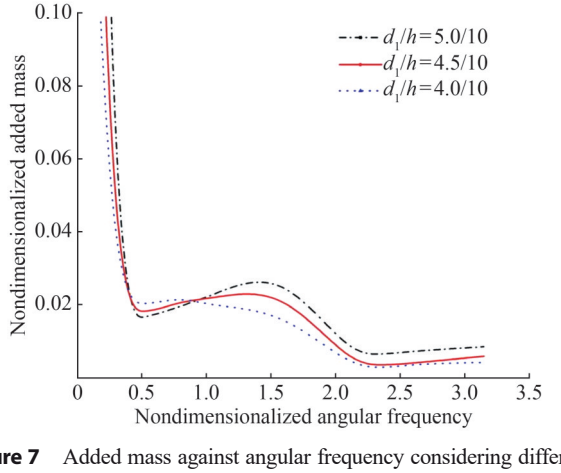

Figure 7 Added mass against angular frequency considering different draft (d_1) values ($\gamma = 0.97$, $b = (5/10)\ h$, $h_1 : h_2 = 7 : 3$, $d_2 = (8/10)\ h$)

tion in pitch motion, has a higher density; that is, the value of γ is higher. The added mass exhibits high values at low frequencies and small density ratios, especially when the cylinder encounters additional water. However, Figure 10 shows that the damping coefficient is substantial when the

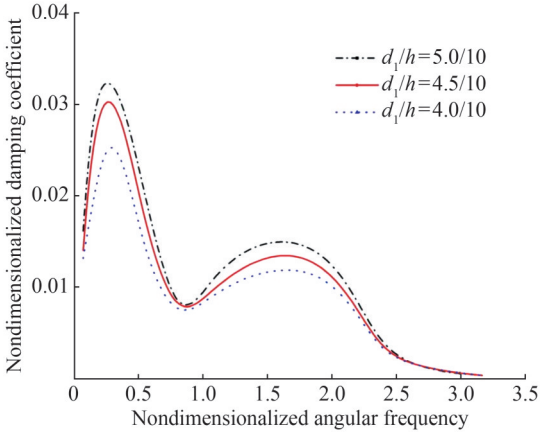

Figure 8 Damping coefficient against angular frequency considering different draft (d_1) values ($\gamma = 0.97$, $b = (5/10)\ h$, $h_1 : h_2 = 7 : 3$, $d_2 = (8/10)\ h$)

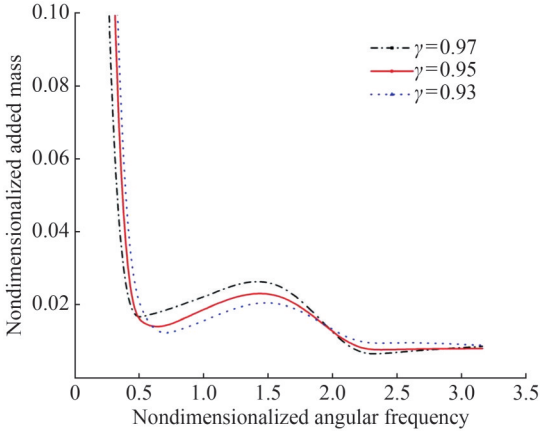

Figure 9 Added mass against angular frequency considering different density ratio (γ) values ($d_1 : d_2 = 5 : 8$, $b = (5/10)\ h$, $h_1 : h_2 = 7 : 3$)

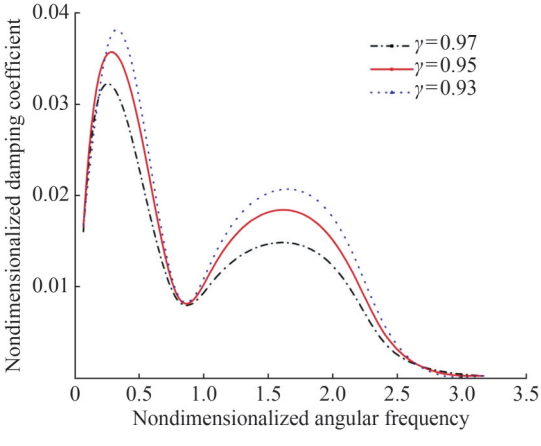

Figure 10 Damping coefficient against angular frequency taking into account different density ratio (γ) values ($d_1 : d_2 = 5 : 8$, $b = (5/10)\ h$, $h_1 : h_2 = 7 : 3$)

density proportion is minimal, and increased disturbance occurs in the flow.

All studies discussed thus far have observed that added

mass is high at low frequencies and decreases at high frequencies. At low frequencies, the damping coefficient shows a sharp oscillatory tendency; at high frequencies, this coefficient approaches zero.

Eqs. (54)–(57) enables the graphical presentation of reflection and transmission coefficients in terms of certain parameters. Figure 11 shows the reflection and transmission coefficients with respect to the wave mode corresponding to $k_0^{(1)}$ due to the incident wave of surface wave mode. In contrast, Figure 12 represents the same with respect to the wave mode corresponding to $k_0^{(2)}$ against nondimensionalized frequency for different draft (d_1) values, that is, d_1/h = 5/10, 4.5/10, 4/10. In both cases, the other parameters are considered: $\gamma = 0.97$, $b = (5/10)h$, $h_1{:}h_2$ = 7:3 and $d_2 = (8/10)h$. Figures 11 and 12 indicate that reflection coefficients increase for structures with larger drafts, whereas transmission coefficients follow an opposite trend.

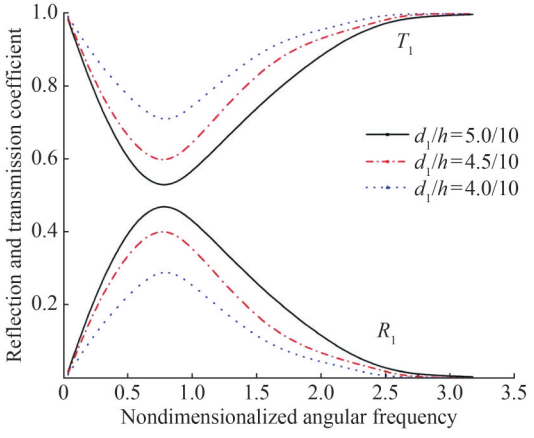

Figure 11 Reflection (R_1) and transmission coefficients (T_1) against angular frequency for wave mode $k_0^{(1)}$ due to the incident wave of surface wave mode with different drafts ($\gamma = 0.97$, $b = (5/10)\,h$, $h_1 : h_2$ = 7:3, $d_2 = (8/10)\,h$)

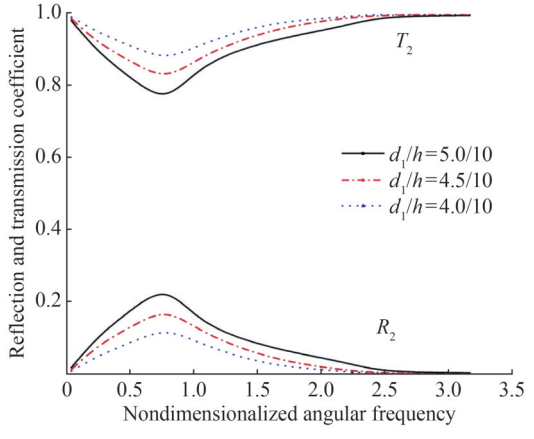

Figure 12 Reflection (R_2) and transmission coefficients (T_2) against angular frequency for wave mode $k_0^{(2)}$ due to the incident wave of surface wave mode with different drafts ($\gamma = 0.97$, $b = (5/10)\,h$, $h_1 : h_2$ = 7:3, $d_2 = (8/10)\,h$)

6 Conclusion

This study focused on a two-layer fluid system comprising a rigid bottom and an open surface on top. Two geometrical structures are considered: one is a bottom-mounted cylinder positioned in the lower fluid layer, and the other is a submerged cylinder in the upper fluid layer. The pitch radiation wave is produced by the rotating pitch oscillations of the submerged cylinder around the y-axis. The mathematical solution for the pitch radiating potential is derived by conducting the separation of variables and the eigenfunction expansion approach. These methods have two primary limitations: i) these methods can be applied only in the linear and homogeneous partial differential equations; ii) these methods are optimal only for simple geometrical structures. The pitch oscillatory motion in this type of two-layer fluid system results in two separate radiation wave modes, namely, the surface- and internal-wave modes on the open surface and interface, respectively. The effects of density proportion between the fluid layers are discussed, and numerical results of hydrodynamic coefficients, that is, added mass and damping coefficient, are graphically illustrated for numerous values throughout a frequency range. These findings demonstrate that density stratification in a two-layer fluid system affects the damping coefficient and added mass of an oscillatory body. The hydrodynamic forces influence the movement of the floating cylinder. The device investigated in this study can be regarded as a point absorber, which comprises a cylindrical buoyant section that moves relative to a mounted caisson. The hydrodynamic forces also induce movement to the buoyant section. This movement relative to the base is converted to mechanical energy using hydraulic pumps or mechanical linkages. Mechanical energy is transferred to a generator or hydraulic system. In hydraulic systems, the movement drives a hydraulic pump, and the pressure of the hydraulic fluid can be used to drive a turbine or generator. These hydraulic cylinders or generators are employed for electric energy production. Therefore, the physical factors examined in this study should be considered when creating or designing an efficient wave energy device that can extract the maximum amount of power. Several promising directions are presented for future development of this work:

i) The present study could be extended by considering different radii for both cylinders, introducing a new research problem.

ii) The solid cylinders investigated in this study could be replaced with porous structures.

iii) The entire study is based on linear water wave theory. Thus, future research could explore the nonlinear case.

Funding This work was supported by MHRD as researcher C. K. Neog received the MHRD Institute GATE scholarship from Govt. of India.

Competing interest The authors have no competing interests to declare that are relevant to the content of this article.

References

Abbas Z, Altaf I, Hasnain J, Ali A (2021) Theoretical analysis of two-layer fluids with continuity of stresses at interface and slip at the walls of an inclined channel. Ain Shams Engineering Journal 12(1): 761-774. https://doi.org/10.1016/j.asej.2020.09.002

Baines PG (1995) Topographic effects in stratified flows. Cambridge university press

Barman KK, Chanda A, Tsai CC (2023) A mathematical study of a two-layer fluid flow system in the presence of a floating breakwater in front of VLFS. Applied Mathematical Modelling 122: 706-730. https://doi.org/10.1016/j.apm.2023.06.017

Bhatta DD, Rahman M (2003) On scattering and radiation problem for a cylinder in water of finite depth. International Journal of Engineering Science 41(9): 931-967. https://doi.org/10.1016/S0020-7225(02)00381-6

Cadby JR, Linton CM (2000) Three-dimensional water-wave scattering in two-layer fluids. Journal of Fluid Mech 423: 155-173. http://doi.org/10.1017/S0022112000002007

Das D (2015) Construction of wave-free potentials and multipoles in a two-layer fluid having free-surface boundary condition with higher-order derivatives. J. Marine Sci. Appl 14(3): 270-282. http://doi.org/10.1007/s11804-015-1321-y

Das D, Mandal BN (2007) Wave scattering by a horizontal circular cylinder in a two-layer fluid with an ice-cover. International Journal of Engineering Science 45(10): 842-872. https://doi.org/10.1016/j.ijengsci.2007.05.008

Das D, Mandal BN (2010) Wave radiation by a sphere submerged in a two-layer ocean with an ice-cover. Applied Ocean Research 32(3): 358-366. https://doi.org/10.1016/j.apor.2009.11.002

Du T, Wu W (2001) The generation and distribution of ocean internal waves. MARINE SCI.-QING.-CHIN. ED. 25(4): 25-27

Koo, W (2010) Free surface simulation of a two-layer fluid by boundary element method. International Journal of Naval Architecture and Ocean Engineering 2(3): 127-131. https://doi.org/10.2478/IJNAOE-2013-0028

Linton CM, McIver M (1995) The interaction of waves with horizontal cylinders in two-layer fluids. Journal of Fluid Mech 304: 213-229. http://doi.org/10.1017/S002211209500440X

Linton CM, McIver P (2001) Handbook of mathematical techniques for wave/structure interactions. Chapman and Hall/CRC

Martha SC, Bora S (2007) Reflection and transmission coefficients for water wave scattering by a sea-bed with small undulation. ZAMM- Journal of Applied Mathematics and Mechanics/Zeitschrift f˙ur Ange-wandte Mathematik und Mechanik 87(4): 314-321. https://doi.org/10.1002/zamm.200610317

Mohapatra S, Bora SN (2010) Radiation of water waves by a sphere in an ice-covered two-layer fluid of finite depth. Journal of Advance Research in Applied Mathematics 2(1): 46-63. http://doi.org/10.5373/jaram.241.102009

Mohapatra S, Bora SN (2011) Reflection and transmission of water waves in a two-layer fluid flowing through a channel with undulating bed. ZAMM-Journal of Applied Mathematics and Mechanics/Zeitschrift für Angewandte Mathematik und Mechanik 91(1): 46-56. https://doi.org/10.1002/zamm.200800216

Mohapatra SC, Da Silva Bispo IB, Guo Y, Guedes SC (2024) Analysis of Wave-Induced forces on a floating rectangular box with analytical and numerical approaches. Journal of Marine Science and Application 23(1): 113-126. https://doi.org/10.1007/s11804-024-00385-7

Mondal R, Sahoo T (2012) Wave structure interaction problems for two-layer fluids in three dimensions. Wave Motion 49(5): 501-524. https://doi.org/10.1016/j.wavemoti.2012.02.002

Neog CK, Hassan M (2023) Evaluation of exciting force and moment by a vertical floating cylinder in appearance of a coaxial cylindrical obstacle in two-layer fluid. Journal of Engineering Mathematics 141(1): 5. http://doi.org/10.1007/s10665-023-10280-9

Neog CK, Hassan M (2024) Hydrodynamic of surge radiation by a floating cylinder in the presence of bottom-mounted cylindrical obstacle in a two-layer fluid system. Journal of Engineering Mathematics 145(1): 1-26. https://doi:10.1007/s10665-024-10339-1

Shah KS, Pegler SS, Minchew BM (2021) Two-layer fluid flows on inclined surfaces. Journal of Fluid Mechanics 917: A54. https://doi.org/10.1017/jfm.2021.273

Shen YM, Zheng YH, You YG (2005) On the radiation and diffraction of linear water waves by a rectangular structure over a sill. Part I. Infinite domain of finite water depth. Ocean Engineering 32(8-9): 1073-1097. https://doi.org/10.1016/j.oceaneng.2004.07.011

Sherief HH, Faltas MS, Saad EI (2003) Forced gravity waves in two-layered fluids with the upper fluid having a free surface. Canadian Journal of Physics 81(4): 675-689. https://doi.org/10.1139/p02-133

Shi Q, You YX, Miao GP (2008) Diffraction of water waves by a vertically floating cylinder in a two-layer fluid. China Ocean Engineering 22(2): 181-193

Shi Q, You YX, Miao GP (2009) Radiation of vertically floating cylinder in two-layer fluid. Journal of Shanghai Jiaotong University 43(2): 187-192

Shi Q, You YX, Wei G, Miao GP (2006) The interaction of water waves with a floating rectangular box in a two-layer fluid. Progress in Natural Science 16(8): 992-1001

Sturova IV (1999) Problems of radiation and diffraction for a circular cylinder in a stratified fluid. Fluid dynamics 34(4): 521-533

Ten I, Kashiwagi M (2004) Hydrodynamics of a body floating in a two-layer fluid of finite depth. Part 1. Radiation problem. Journal of Marine Science and Technolgy 9: 127-141. https://doi.org/10.1007/s00773-004-0185-7

Wu BJ, Zheng YH, You YG, Jie DS, Chen Y (2006) On diffraction and radiation problem for two cylinders in water of finite depth. Ocean Engineering 33(5-6): 679-704. http://doi.org/10.1016/j.oceaneng.2005.05.011

Wu BJ, Zheng YH, You YG, Sun XY, Chen Y (2004) On diffraction and radiation problem for a cylinder over a caisson in water of finite depth. International Journal of Engineering Science 42(11-12): 1193-1213. https://doi.org/10.1016/j.ijengsci.2003. 12.006

Xu F, Lu DQ (2010) Wave scattering by a thin elastic plate floating on a two-layer fluid. International Journal of Engineering Science 48(9): 809-819. https://doi.org/10.1016/j.ijengsci.2010.04.007

You YX, Shi Q, Miao GP (2005) The hydrodynamic forces on a large diameter cylinder in Two-Laver fluid. Shanghai Jiaotong Daxue Xuebao (J. Shang. Jiaotong Uni.) (China) 39(5): 695-700

You YX, Shi Q, Miao GP (2007) The radiation and diffraction of water waves by a bottom-mounted circular cylinder in a two-layer fluid. Journal of Hydrodynamics 19(1): 1-8. https://doi.org/10.1016/S1001-6058(07)60020-1